Quantum target ranging for LiDAR

Letter

Quantum target ranging for LiDAR

Giuseppe Ortolano [1,2,3] and Ivano Ruo-Berchera [1]

[1] *Quantum Metrology and Nano Technologies Division, INRiM, Strada delle Cacce 91, 10153 Torino, Italy*
[2] *Dipartimento di Fisica e Astronomia, Università di Firenze, Via G. Sansone 1, I-50019 Sesto Fiorentino (FI), Italy*
[3] *Istituto Nazionale di Fisica Nucleare, Sezione di Firenze, Via G. Sansone 1, I-50019 Sesto Fiorentino (FI), Italy*

(Received 7 August 2024; revised 20 October 2024; accepted 30 April 2025; published 9 June 2025)

We investigate Quantum Target Ranging in the context of multihypothesis testing and its applicability to real-world LiDAR systems. First, we demonstrate that ranging is generally an easier task compared to the well-studied problem of target detection. We then analyze the theoretical bounds and advantages of quantum ranging in the context of phase-insensitive measurements, which is the operational mode of most LiDAR systems. Additionally, we adopt a background noise model more suited to optical frequencies, as opposed to the typical single-mode thermal noise model used in quantum target detection theory. Our findings indicate that a significant exponential quantum advantage can be achieved using simple photon-counting receivers across a broad range of parameters, thereby validating the efficacy of the quantum approach for LiDAR implementations.

DOI: 10.1103/PhysRevResearch.7.L022059

In the context of quantum sensing [1–10], improving target detection and ranging by leveraging quantum correlations and entanglement has received large attention in the last 15 years [11–15], stemming from the proposal of the quantum illumination (QI) protocol [16,17]. This huge interest is justified by the perspective of a potential disruptive advancement of the radar and LiDAR technology [18,19], widely used in surveillance, both civil and military aviation, automotive, environment monitoring, and even biological imaging [20].

The problems of quantum target detection (QTD) and ranging (QTR) are closely related. In QTD one uses a probe state to asses whether a target is present or not at a given *a priori* position. On the other hand, in QTR one assumes that the object is present and tries to localize it. It is clear that any real-world application would most likely need to address both tasks.

For the detection problem schematically represented in Fig. 1(a), Tan *et al.* [21] showed that 6 dB of quantum advantage can be obtained in the exponent of error probability decay with the number of probe usages L when compared to the optimal classical case. The latter is given by a coherent transmitter paired with homodyne detection. The most intriguing thing is that this advantage is obtained in highly "hostile" conditions: small mean signal photon number $\mu \ll 1$, large mean background $\mu_B \gg 1$, and low target reflectance $\kappa \ll 1$, a regime where delicate quantum states are typically not expected to be useful.

Despite a large number of theoretical [22–26] and experimental studies [27–30], the challenges in the realization of an optimal receiver [31,32], the decoherence-free storage of the ancillary modes, and the required large time–bandwidth product of the transmitter still make QI inconvenient in practical scenarios.

Surprisingly, only recently has the problem of QTR been addressed [26]. This problem can be tackled in different related formalisms: as an estimation problem, establishing the ultimate range-delay accuracy in a continuous time measurement approach [33]. In the framework of hypothesis testing is the task of determining which of many range-delay resolution bins contains a target that is known to be present in one of them [34,35], as depicted in Fig. 1(b). Those analyses show a quantum enhancement of QTR similar to the QI's one in the same range of parameters, leaving similar concerns on the practical utility.

Many real-world LiDARs for two- and three-dimensional (2D and 3D) applications operate measuring the time of flight just by direct intensity measurement of short time pulses [36]. This is because homodyne detection requires phase-locking of the traveling signal with a local oscillator, which is usually hard in the presence of environmental phase noise, sample roughness, and without information on the object distance. Also heterodyne-detention-based LIDAR, although to a lesser extent, suffers similar issues [37]. Phase-insensitive measurements are more and more practical and efficient, especially now that single photon detector technology has few ps jitter [38], corresponding to submillimeter resolution in space [39]. Thus, in many practical cases, the optical classical coherent receiver benchmark may become too restrictive; rather, it makes sense to compare quantum and classical ranging schemes limited to phase-insensitive measurements using direct photon-counting (PC) receivers [40,41]. Note that photon counting paired with coherent transmitters, being able to access the photon statistics, can provide an advantage with respect to mean intensity measurement–based LiDAR [42]. Along the same spirit, the usual QI theoretical model for the noise that combines coherently a highly populated

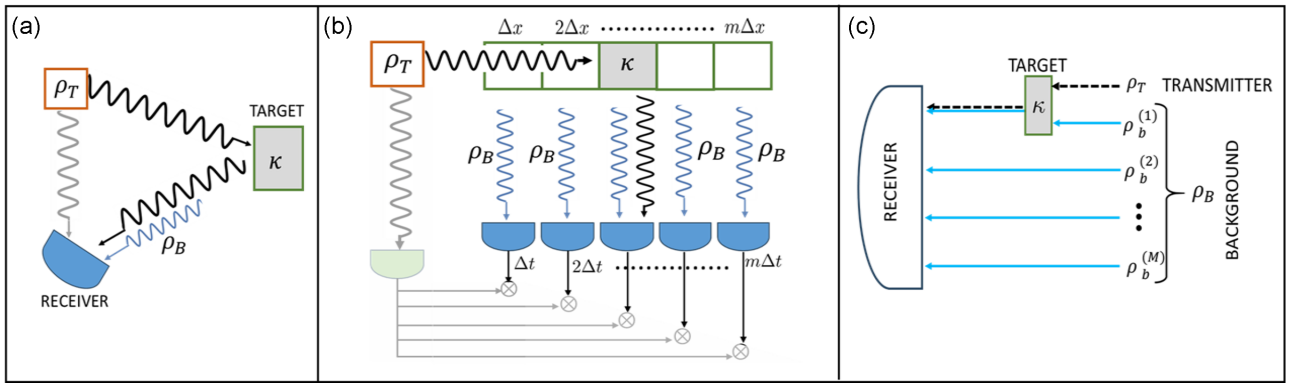

FIG. 1. *Sensing and detention schemes.* (a) QTD: A signal mode in the state ρ_T interacts with a target of reflectance κ and reflected back at the receiver immersed in a background. An ancillary mode (in faint color) correlated with the signal may be used in a joint measurement. (b) QTR: the target is in one among m longitudinal space slots of size Δx. The returning signal arrives in a certain corresponding temporal time bin, while the other bins only detect background. An ancillary-assisted strategy, exploiting a bipartite state and postprocessing correlation measurements, may be used, represented in fainted colors. (c) Uncorrelated noise model: Each receivers intercepts a large number $M \gg 1$ of low-mean-photon-number background modes. In this limit the noise and the probe photon statistics are approximated as independent.

single-mode thermal state with the transmitted probe mode in a beam-splitter-like model is more suited for the microwave regime rather than for the optical domain where blackbody thermal radiation is negligible at operating temperatures, and other sources of noise, like sun irradiance, with very low coherence times (of the order of fs) contribute. Thus, here we consider the QTR problem with a different model of noise background as represented in Fig. 1(c), where the detector integrates over a large number of independent optical background modes (both temporal and spatial modes within the integration area and time of the detector) and the signal couples with just one or a comparatively small number of them, randomly. The mean photon number for each background mode is usually small so that it can be considered in the limit of Poisson photon statistics.

QTD with PC measurements has been previously considered in literature [14,43–45]; however, while strong time correlation in the photon entangled pairs is used to reduce the background effect, the classical transmitter typically lacks any narrow-temporal synchronization with the detectors, inhibiting any possibility of time filtering of the noise through time gating. Referring to Fig. 1(b), in this work we consider the time resolution Δt as fixed, for example, set by the detector time bin (or jitter) and both quantum correlation coherence time and classical single-shot signal pulse duration shorter than Δt. This ensures a fair comparison. Our analysis can be expanded to schemes involving multiplexed frequency detection to further reduce the noise contribution [46,47].

The model. The scheme of target detection is shown in Fig. 1(a). A transmitter probe state ρ_T is sent to detect a given partially reflecting target. A measurement is performed at the receiver on the returning signal state ρ_R. The target is immersed in a background in the state ρ_B with mean photon number μ_B. The effect of the signal interaction with the target and the background modes is described by a noisy and lossy channel $\mathcal{E}_{\kappa,\mu_B}$, where κ is the reflectance of the target. The resulting state at the receiver is $\rho_\kappa = \mathcal{E}_{\kappa,n_B}(\rho_T)$. In particular, if the target is absent, i.e., $\kappa = 0$, only the background reaches the detector, so the final state is $\rho_{\kappa=0} = \rho_B$. Target detection is formally described as a binary hypothesis testing problem with hypotheses $\mathcal{H}_1 : \rho_R = \rho_\kappa$ and $\mathcal{H}_0 : \rho_R = \rho_B$, where hereinafter ρ_κ is intended with $\kappa \neq 0$.

On the other hand, in target ranging, the measurements are performed on m time slots as depicted in Fig. 1(b). Since the modes in each time slot are considered independent, denoting as $\mathcal{H}_j$ the hypothesis of the target in the jth time slot, the ranging becomes an m-ary hypotheses testing problem among $\{\mathcal{H}_1, ..., \mathcal{H}_m\}$ defined through the corresponding output states,

$$\mathcal{H}_j : \rho_R = \rho_j := \rho_\kappa^{(j)} \bigotimes_{i\neq j}^{m-1} \rho_B^{(i)}, \tag{1}$$

where $\rho^{(i)}$ is the state of the ith time slot.

This formulation for the ranging problem assumes that the target is present in one and only one bin. Other definitions of ranging could be analyzed with the same formalism by modifying the hypotheses set, for example, by adding hypotheses contemplating more than one target or no target at all, but their analysis is beyond the scope of our work.

QTR: Relation with QTD. Clearly, detection and ranging are different tasks; nevertheless, we can derive a connection between them, which holds independently from the particular input states ρ_T and form the interaction channel $\mathcal{E}_{\kappa,\mu_B}$ that can be either the conventional single-mode beam-splitter-like mixing with a thermal noise contemplated in literature or our multimode optical noise channel of Fig. 1(c).

We characterize the relation between QTR and QTD in the asymptotic regime of multicopy states, where the exponential decay rate of the probability of error in a quantum hypothesis testing is given by the quantum Chernoff information [48]. In the asymptotic regime the decay rate of the probability of error in multihypotheses testing is the same as the binary one of the two "closest" hypotheses in the set [49] and is thus independent of the number m of hypotheses, making a comparison between detection and ranging fair. We detail our analysis in the Appendix.

Our results give a direct relation between the quantum Chernoff information of target ranging, ξ_{TR}, and the quantum

Bhattacharya information of target detection, $\mathcal{B}_{\rm TD}$:

$$\xi_{\rm TR} = 2\mathcal{B}_{\rm TD} \geqslant \xi_{\rm TD}. \tag{2}$$

On the right-hand side, $\xi_{\rm TD}$ denotes the quantum Chernoff information of target detection, and the inequality follows from the concavity of the α information (see Appendix). Equation (2) states that asymptotically the task of ranging, given previous knowledge on the presence of the target, can be performed with better accuracy than target detection, regardless of the number of time slots m considered. This result is completely general, meaning that it does not depend on the form of the probe states and on the kind of measurement performed.

QTR: Phase-insensitive measurement. As explained in the Introduction, now we focus on the research of the quantum advantage when considering phase-insensitive PC measurement, for both classical and quantum states of the transmitter at a fixed number of signal photons per single use of the probe or equivalently, at a fixed probe power (i.e., photon energy divided by Δt). In particular, we will compare the performance of a coherent transmitter $\rho_T = \rho_{\rm coh}$, acting as a classical benchmark, with the nonclassically correlated bipartite state $\rho_T = \rho_Q$ defined in the following. Note that since we are fixing the power rather than the total energy, the Chernoff information is enough to characterize the best classical performance. We do not expect classical correlation to outperform the coherent transmitter in this context (see our analysis in the Supplemental Material (SM) [60]). The QTR is performed using a multicopy transmitter's state of the form $\rho_T^{\otimes L}$. Fixing the measurements to photon counting yields a classical hypothesis testing. Its optimal asymptotic probability of error decay rate is given by the classical Chernoff information [50]. In the Appendix we cover this problem in more detail and we show for the classical Chernoff information a similar result to that already presented in Eq. (2) for the quantum case, $\xi_{\rm TR}^{\rm cla} = 2\mathcal{B}_{\rm TD}^{\rm cla}$.

We denote quantities with the superscript "cla" to indicate that they refer to Chernoff, Bhattacharya and α information of probability distributions after fixing the measurement to PC, i.e. the classical version of the previously defined quantities for quantum states. In the following we will omit the superscript for brevity of notation. In our model for the noise, we always assume that the background can be approximated having a Poisson distribution, $P_B(n) = \mathcal{P}_{\mu_B}(n)$, and the statistics of the photo-counts in the only slot receiving the probe's photons is the convolution of the background noise with the signal, i.e they sum up incoherently. For the coherent state transmitter, $\rho_T = \rho_{\rm coh}$, the probe's distribution is also a Poissonian $\mathcal{P}_\mu$, so that $P_\kappa(n) = \mathcal{P}_{\mu_B} * \mathcal{P}_{\kappa\mu}$ ('$*$' stands for convolution). In this case, the Chernoff information of the target ranging task, can be found analytically, as reported in the SM [60], as

$$\xi_{\rm coh} = \kappa\mu + 2\mu_B - 2\sqrt{\mu_B}\sqrt{\mu_B + \kappa\mu}, \tag{3}$$

where μ is the mean number of photons in the probe state ρ_T and μ_B is the mean number of background photons.

The quantum probe that we will consider is a collection of a large number of two mode squeezed vacuum (TMSV) states, $\rho_Q = (|TMSV\rangle\langle TMSV|)^{\otimes R}$. The TMSV state is defined as $|TMSV\rangle = \sum_n c_n^{\mu_0} |n,n\rangle_{S,I}\langle n,n|$, with $|c_n^{\mu_0}|^2$ a thermal distribution with mean μ_0. This state is entangled and presents perfect correlation between signal and idler photon numbers. Taking R copies of this state preserves the photon number correlation and in the limit of small μ_0 and large R gives a marginal photon-number distribution that is Poissonian instead of the thermal one of the single-copy state [51]. We chose this configuration because a narrower marginal distribution has the potential to provide an advantage in a broader range of parameters [51,52]. Note how in some regimes it may be convenient to use a single-mode TMSV (see SM [60]). For a fair comparison with the coherent case, we set $R\mu_0 = \mu$ so that both probes have the same number of signal photons. The results found above are easily extended to a bipartite system considering the joint distributions of signal and idler in place of the signal one, and ξ_Q for the quantum probe ρ_Q can be computed in terms of the Bhattacharya information of the detection task. The evaluation of ξ_Q is performed numerically.

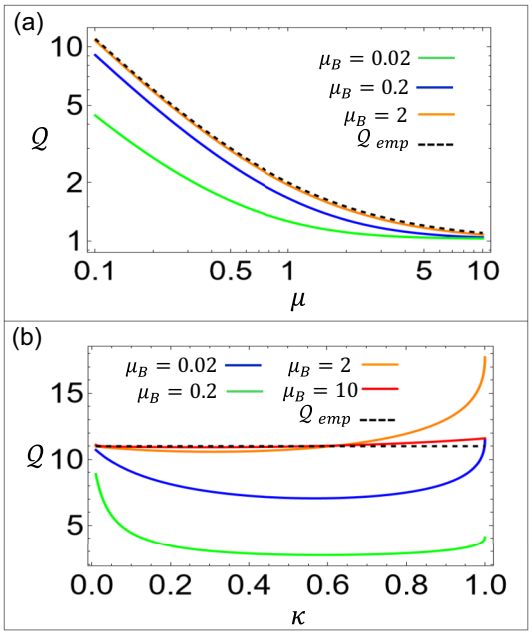

FIG. 2. *Asymptotic quantum advantage.* (a)The quantum advantage $\mathcal{Q}$ defined in the text is plotted against the mean number of probes' photons $\mu(\kappa = 0.1)$. (b)Quantum advantage as a function of κ $(\mu = 0.1)$. Colors represents different values of the background μ_B. The black-dashed line is the empirical limit defined in the text.

In Fig. 2(a) we report the quantum advantage $\mathcal{Q} = \xi_Q/\xi_{\rm coh}$ in the regime of small reflectance $(\kappa = 0.1)$ as a function of the mean number of probe photons μ for different values of background photons $\mu_B = 0.02, 0.2, 2$. Interestingly, it turns out that when $\kappa \ll 1$ and $\mu_B \gg 1$ (in practice, $\mu_B = 2$ seems enough to fulfill the condition) the quantum advantage reaches the empirical bound $\mathcal{Q}_{\rm emp} = 1 + 1/\mu$, represented by the black dashed line. $\mathcal{Q}_{\rm emp}$ corresponds to the square of the ratio among the maximum phase-sensitive field correlation, $\langle a_1 a_2\rangle$, allowed for the quantum, $\sim\sqrt{u(u+1)}$, and classical, $\sim u$, bipartite Gaussian states, which is known to be the origin of the quantum advantage in Gaussian state QI [53]. However, note that in our scheme we do not use the classical benchmark of a correlated classical state, rather a coherent state. Figure 2(a) shows that in general the quantum advantage is

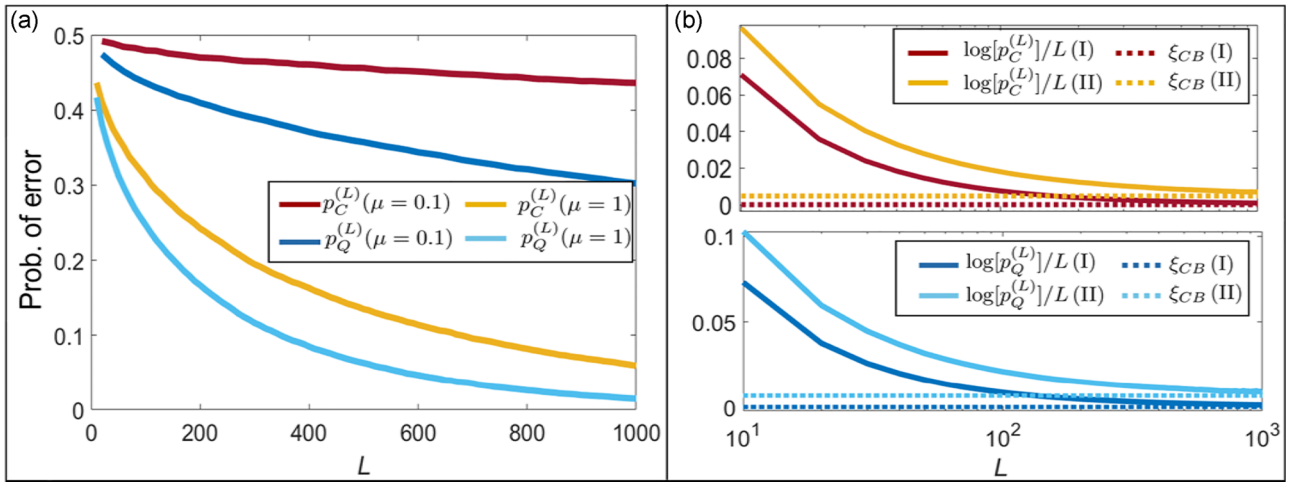

FIG. 3. *Nonasymptotic probabilities of error.* (a) Classical and quantum error probabilities, $p_C^{(L)}$ and $p_Q^{(L)}$, are compared as a function of the number of probes' copies L ($\mu_B = 2, \kappa = 0.1$). (b) Scaling of the logarithmic error probabilities (solid lines), $p_C^{(L)}$ (top panel) and $p_C^{(L)}$ (bottom), and the corresponding Chernoff bound (dotted), for two sets of parameters: (I) $\mu_B = 2, \mu = 2, \kappa = 0.1$, and (II) $\mu_B = 1, \mu = 0.1, \kappa = 0.1$.

significant in the region of $\mu \ll 1$, eventually approaching $\mathcal{Q} = 1$, i.e., no advantage, in the opposite regime. Figure 2(b) shows that the dependence of $\mathcal{Q}$ from the target reflectance κ has a nontrivial behavior, only for $\mu = 10 \gg 1$ (the red curve) the Q dependence from κ is negligible. In the other situation, the highest advantage is found in the two extreme regions of either very high or very low reflectance. The low-reflectance regime $\kappa \ll 1$ is the one providing an advantage in the conventional model of quantum illumination, while the high-reflectance regime, $\kappa \gg 1$, is where the quantum reading protocol [51,52,54,55] finds the best quantum gain. The asymptotic behavior of the probability of error gives no information about the dependence on the number m of time slots. This dependence can be derived by setting an optimal postprocessing strategy to compute the exact probability of error. We address the dependence on m in the Appendix.

QTD: Nonasymptotic quantum advantage. The nonclassically correlated probe ρ_Q introduced in the asymptotic analysis of $L \gg 1$ is unable to outperform the coherent state transmitter in ranging in the single-copy scenario with photon counting. This is due to the fact that knowledge of the idler does not change the optimal Bayesian decision, which remains to pick the higher signal count regardless of the idler. In other words, in the single-shot ranging with photon counting, the performance depends only on the marginal signal photon number statistic. Thus a quantum advantage in this scenario can be obtained by a probe with sub-Poisson marginal distribution, such as the one in a Fock state.

In this section we will instead consider a finite number L of repetitions and explore the advantage of ρ_Q in this nonasymptotic regime, which is arguably of the most practical interest. The outcome of the PC measurement in QTR scheme of Fig. 1(b), with the input state $\rho_Q^{\otimes L}$, is an array $\tilde{\mathbf{n}}_S = \{\tilde{\mathbf{n}}_1, ..., \tilde{\mathbf{n}}_m\}$ for the signal, with each $\tilde{\mathbf{n}}_j$ being L-dimensional vectors of integers. For the idler the outcome is a single L-dimensional vector $\tilde{\mathbf{n}}_I = \{\tilde{n}_I^{(1)}, ..., \tilde{n}_I^{(L)}\}$, with $\tilde{n}_I^{(i)}$ scalar integers. In the following we show that an asymptotically optimal decision rule, at least for a small number of photons and dominant background, is to consider for each of the m slots the scalar product $c_j := \tilde{\mathbf{n}}_j \cdot \tilde{\mathbf{n}}_I$ and select as an outcome the slot $\tilde{j} = \arg\max c_j$. A similar strategy for PC-based QDR is known to be optimal [40]. The probability of error of this strategy can be evaluated with numerical analysis, and we denote it as $p_Q^{(L)}$.

On the other hand, for a coherent probe in the state ρ_C the best strategy for an L-copy state is to select the time slot with the highest total count after summing on the L copies. In other words, for a probe consisting of L copies of a coherent state each with μ mean photons achieves the same performance of a single coherent state with $L\mu$ mean photons and a total background $L\mu_B$. It follows that the nonasymptotic multicopy optimal probability of error is $p_C^{(L)}(\mu, \mu_B) = p_C^{(1)}(L\mu, L\mu_B)$.

In Fig. 3(a) we compare the probabilities of error $p_C^{(L)}$ and $p_Q^{(L)}$ as a function of L, showing that a sensible quantum advantage can be found also in the nonasymptotic regime. Just for simplicity and without loss of generality, we refer to the case $m = 2$. The comparison is shown for two values of the probe mean photon number ($\mu = 0.1$ and $\mu = 1$) while the other parameters are kept fixed. In Fig. 3(b) we plot the logarithm of the error probabilities normalized to L (solid lines) to show that they approach asymptotically the corresponding Chernoff information ξ_Q and ξ_{coh} (dashed lines). Thus, the Chernoff bounds being asymptotically tight, the corresponding practical decision strategies are asymptotically optimal. In this work we have shown that QTR is in general an easier task than QTD. Calculating the optimal bounds to the error probability in the asymptotic regime for phase-insensitive measurement, we have found that QTR with an entangled transmitter can achieve an exponent advantage inversely proportional to the mean photon number for a single use of the probe with respect to the best classical transmitter if both are paired with a PC receiver. Simple photon number correlationlike measurement is asymptotically optimal, and its advantage persists also in the nonasymptotic case. Our analysis represents a significant step in the analysis towards a real implementation of quantum LiDAR.

Acknowledgments. This project has received funding from the European Defence Fund (EDF) under Grant Agreement No. 101103417 EDF-2021-DIS-RDIS-ADEQUADE. Funded by the European Union. Views and opinions expressed are, however, those of the authors only and do not necessarily reflect those of the European Union or the European Commission. Neither the European Union nor the granting authority can be held responsible for them.

The work has also received funding from Next Generation EU, Missione 4 Componente 1 CUP C63C22000830006 - Bando a Cascata Spoke Fondazione Bruno Kessler-M4C2I.1.3-NQSTI.

G.O. acknowledges funding from the European Union under the Piano Nazionale di Ripresa e Resilienza (PNRR) of NextGenerationEU, a partnership on "Telecommunications of the Future" (PE00000001 - program "RESTART").

Both the authors conceived the scheme of QTR paired with the PC receiver. G.O. elaborated the theory and performed calculations and simulations. Both authors contributed to the paper writing. I.R.-B. is responsible for the funding.

The authors declare no competing interest.

Data availability. All data needed to evaluate the conclusions are reported in the paper. Further data are available under reasonable request to the corresponding author.

Appendix.

1. Relation between detection and ranging. Given a binary hypothesis problem $\mathcal{H}_0/\mathcal{H}_1$ characterized respectively by the corresponding final states ρ_0/ρ_1 occurring with the corresponding prior probabilities $\pi_0 + \pi_1 = 1$, the probability of error is given by the Helstrom bound [56].

Consider now a sensing performed with a multicopy input state $\rho_T^{\otimes L}$, where the transmission channel $\mathcal{E}_{\kappa,\mu_B}$ is assumed to act independently on each copy. In this multicopy case the Helstrom bound can be difficult to compute. However, in the asymptotic regime of $L \to \infty$, a useful upper limit to the optimal probability of error is given by the quantum Chernoff bound:

$$p_{\text{err}}\left(\rho_0^{\otimes L}, \rho_1^{\otimes L}\right) \leqslant \tfrac{1}{2} e^{-\xi_{\text{QCB}} L}, \tag{A1}$$

where we fixed $\pi_i = 1/2$, meaning that no prior information is available. The bound in Eq. (A1) is tight in the error exponent for $L \gg 1$ [48]. Here, ξ_{QCB} is the *quantum Chernoff information* [48], defined as

$$\xi_{\text{QCB}}(\mathcal{H}_0, \mathcal{H}_1) := \max_{\alpha\in[0,1]} C_\alpha(\rho_0, \rho_1), \tag{A2}$$

i.e., by the maximization of the α information, C_α, between the single-copy states ρ_0 and ρ_1: $C_\alpha(\rho_0, \rho_1) := -\log(\text{Tr}[\rho_0^\alpha \rho_1^{1-\alpha}])$. C_α is concave in α over the interval $\alpha \in [0, 1]$. Notably, in the asymptotic limit $L \gg 1$, the exponential decay rate for a set of m hypotheses $\{\mathcal{H}_1, ..., \mathcal{H}_m\}$, ξ^m, is equal to [49]

$$\xi_{\text{QCB}}^{(m)} = \min_{i,j} \xi_{\text{QCB}}^{(2)}(\mathcal{H}_i, \mathcal{H}_j). \tag{A3}$$

This relation has been proven for finite-dimensional Hilbert spaces, and it holds in our analysis due to the assumption that the sensing is performed at a finite fixed energy μ, meaning that the states can be projected to a finite-dimensional truncated space [57]. In other words, in the asymptotic regime, the exponential decay rate of multihypotheses testing is the same as the binary one of the two "closest" hypotheses in the set. Thus, it makes sense to compare QTR and QTD in this limit. For the symmetry of the states in Eq. (1), we can arbitrarily chose two hypotheses of the set to substitute in Eq. (A3), obtaining by Eq. (A2),

$$\begin{aligned}\xi_{\text{TR}} &= \max_{\alpha\in[0,1]} C_\alpha\left(\rho_\kappa \otimes \rho_B \bigotimes^{m-2} \rho_B, \rho_B \otimes \rho_\kappa \bigotimes^{m-2} \rho_B\right)\\ &= \max_{\alpha\in[0,1]} C_\alpha(\rho_\kappa \otimes \rho_B, \rho_B \otimes \rho_\kappa)\\ &= 2\,C_{1/2}(\rho_\kappa, \rho_B) := 2\mathcal{B}_{\text{TD}} \geqslant C_\alpha(\rho_\kappa, \rho_B),\end{aligned} \tag{A4}$$

where we introduced the quantum Bhattacharya information for target detection $\mathcal{B}_{\text{TD}}$. The first equality follows from discarding additional systems in a tensor product that are the same under both hypotheses, and the last equality is demonstrated in the SM [60]. Note that C_α is symmetrical at $\alpha = 1/2$, i.e., $C_{1/2}(\rho_\kappa, \rho_B) = C_{1/2}(\rho_B, \rho_\kappa)$. The last inequality derives directly from the concavity of the α information.

2. Photon counting: Classical Chernoff information. In this paragraph we address the case of measurement fixed to photon counting. Initially, let us consider ρ_T a single-mode state addressed to the target. For the target in the jth time slot, the single-copy state at the receiver ρ_j is given in Eq. (1). Given $|n_i\rangle$ the eigenstate with eigenvalue n_i of the number operator $\hat{n}_i = \hat{a}_i^\dagger \hat{a}_i$ of the field in the ith slot and defining the multimode Fock state $|\mathbf{n}\rangle = \bigotimes_i |n_i\rangle$, the photocounts probability distribution is then, $P_j(\mathbf{n}) = \text{Tr}(\rho_j |\mathbf{n}\rangle\langle\mathbf{n}|)$. The best-ranging performance will depend on the set of classical probability distributions $\{P_1(\mathbf{n}), ..., P_m(\mathbf{n})\}$, corresponding to a classical m-hypotheses test on the set of measurement outcomes. The probability of error decays exponentially with L at the rate fixed by the so-called *classical Chernoff information* $\xi_{\text{CB}}^{(m)}$. Similarly to the measurement-independent (quantum) case of Eq. (A3), the m-ary problem can be reduced to a binary test, where [58]

$$\xi_{CB}^{(m)} = \min_{i,j} \xi_{CB}(P_i(\mathbf{n}), P_j(\mathbf{n})). \tag{A5}$$

The binary classical Chernoff information is defined as [50,59]

$$\xi_{\text{CB}}(P_i, P_j) := \max_{\alpha\in[0,1]} -\log\left(\sum_{\mathbf{n}} P_i(\mathbf{n})^\alpha P_j(\mathbf{n})^{1-\alpha}\right). \tag{A6}$$

Following the notation used for the states, let us label P_B and P_κ the photon number distributions at a given time slot, with only background or background plus returning signal, respectively. Following similar steps used to derive Eq. (A4), starting from Eq. (A6), one gets for the PC quantum target ranging,

$$\xi_{\text{TR}}^{\text{cla}} := \max_{\alpha\in[0,1]} C_\alpha^{\text{cla}}(P_B P_\kappa, P_\kappa P_B) = 2\mathcal{B}_{\text{TD}}^{\text{cla}}. \tag{A7}$$

A detailed derivation of this result is given in the SM [60].

3. QTD: Time slot dependence. Let us consider a single-shot scenario, i.e., let us fix $L = 1$. For a coherent state transmitter the single-shot measurement outcome at the receiver is an array of photon counts $\tilde{\mathbf{n}} = \{\tilde{n}_1, ...\tilde{n}_m\}$ referring to each of the m time slots. Given $\tilde{\mathbf{n}}$ the best Bayesian decision is to select the time slot with the highest photon count [56],

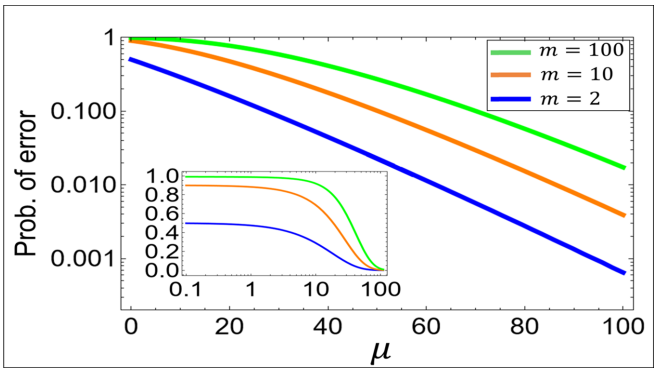

FIG. 4. *Error probability dependence on the number of time slots.* The probability of error $p_C^{(1)}$ is reported as a function of the mean number of transmitted photons μ. The three colors refer to different numbers m of time slots according to the legend (target reflectance $\kappa = 0.1$, mean number of background photons $\mu_B = 1$). The main graph is in linear-log scale, while the insert shows the same functions in log-linear scale.

choosing randomly if the highest count is repeated in more than one slot. This yields the following probability of error (see SM [60]):

$$p_C^{(L=1)}(\mu) = 1 - m^{-1} e^{-\kappa\mu} G_m\left(1 + \kappa \frac{\mu}{\mu_B}\right), \tag{A8}$$

where we introduced the generating function $G_m(x)$:

$$G_m(x) := \sum_{n=0}^{\infty} x^n (Q_{\mu_B}(n+1)^m - Q_{\mu_B}(n)^m),$$

$Q_\mu(n) = \Gamma(n, \mu)/\Gamma(n)$ being the regularized incomplete gamma function.

In Fig. 4 we plot $p_C^{(L=1)}(\mu)$ for different numbers of time slots, $m = 2, 10, 100$. In the main graph, we show the curves in linear-log scale to highlight their similar asymptotic exponential decay rate in the limit of $\mu \gg 1$, which results to be independent from m. Note that in the particular case of coherent states, as discussed in the main text, $p_C^{(L)}(\mu, \mu_B) = p_C^{(1)}(L\mu, L\mu_B)$, thus the asymptotic slope is in fact determined by the Chernoff information.

The insert of Fig. 4 shows, in a different scale, how each curve starts with a probability of error of $1 - 1/m$ at $\mu = 0$, corresponding to a random guess, as expected.

[1] C. L. Degen, F. Reinhard, and P. Cappellaro, Quantum sensing, Rev. Mod. Phys. **89**, 035002 (2017).

[2] S. Pirandola, B. R. Bardhan, T. Gehring, C. Weedbrook, and S. Lloyd, Advances in photonic quantum sensing, Nat. Photon. **12**, 724 (2018).

[3] G. Petrini, E. Moreva, E. Bernardi, P. Traina, G. Tomagra, V. Carabelli, I. P. Degiovanni, and M. Genovese, Is a quantum biosensing revolution approaching? Perspectives in NV-assisted current and thermal biosensing in living cells, Adv. Quantum Technol. **3**, 2000066 (2020).

[4] L. Banchi, Q. Zhuang, and S. Pirandola, Quantum-enhanced barcode decoding and pattern recognition, Phys. Rev. Appl. **14**, 064026 (2020).

[5] M. Barbieri, Optical quantum metrology, PRX Quantum **3**, 010202 (2022).

[6] I. Ruo Berchera, I. P. Degiovanni, S. Olivares, and M. Genovese, Quantum light in coupled interferometers for quantum gravity tests, Phys. Rev. Lett. **110**, 213601 (2013).

[7] I. R. Berchera and I. P. Degiovanni, Quantum imaging with sub-Poissonian light: Challenges and perspectives in optical metrology, Metrologia **56**, 024001 (2019).

[8] G. Ortolano, C. Napoli, C. Harney, S. Pirandola, G. Leonetti, P. Boucher, E. Losero, M. Genovese, and I. Ruo-Berchera, Quantum-enhanced pattern recognition, Phys. Rev. Appl. **20**, 024072 (2023).

[9] J. L. Pereira, L. Banchi, and S. Pirandola, Quantum-enhanced cluster detection in physical images, Phys. Rev. Appl. **19**, 054031 (2023).

[10] G. Ortolano, A. Paniate, P. Boucher, C. Napoli, S. Soman, S. F. Pereira, I. Ruo-Berchera, and M. Genovese, Quantum enhanced non-interferometric quantitative phase imaging, Light Sci. Appl. **12**, 171 (2023).

[11] L. Maccone and C. Ren, Quantum radar, Phys. Rev. Lett. **124**, 200503 (2020).

[12] S. Barzanjeh, S. Guha, C. Weedbrook, D. Vitali, J. H. Shapiro, and S. Pirandola, Microwave quantum illumination, Phys. Rev. Lett. **114**, 080503 (2015).

[13] G. Sorelli, N. Treps, F. Grosshans, and F. Boust, Detecting a target with quantum entanglement, IEEE Aerosp. Electron. Syst. Mag. **37**, 68 (2022).

[14] J. Zhao, A. Lyons, A. C. Ulku, H. Defienne, D. Faccio, and E. Charbon, Light detection and ranging with entangled photons, Opt. Express **30**, 3675 (2022).

[15] R. Gallego Torromé and S. Barzanjeh, Advances in quantum radar and quantum LiDAR, Prog. Quantum Electron. **93**, 100497 (2024).

[16] M. F. Sacchi, Entanglement can enhance the distinguishability of entanglement-breaking channels, Phys. Rev. A **72**, 014305 (2005).

[17] S. Lloyd, Enhanced sensitivity of photodetection via quantum illumination, Science **321**, 1463 (2008).

[18] B. Schwarz, Mapping the world in 3D, Nat. Photon. **4**, 429 (2010).

[19] Y. Hong, S. Liu, Z.-P. Li, X. Huang, P. Jiang, Y. Xu, C. Wu, H. Zhou, Y.-C. Zhang, H.-L. Ren, Z.-H. Li, J. Jia, Q. Zhang, C. Li, F. Xu, J.-Y. Wang, and J.-W. Pan, Airborne single-photon LiDAR towards a small-sized and low-power payload, Optica **11**, 612 (2024).

[20] R. Murray and A. Lyons, Two-photon interference LiDAR imaging, Opt. Express **30**, 27164 (2022).

[21] S.-H. Tan, B. I. Erkmen, V. Giovannetti, S. Guha, S. Lloyd, L. Maccone, S. Pirandola, and J. H. Shapiro, Quantum illumination with Gaussian states, Phys. Rev. Lett. **101**, 253601 (2008).

[22] R. Nair, Discriminating quantum-optical beam-splitter channels with number-diagonal signal states: Applications to quantum reading and target detection, Phys. Rev. A **84**, 032312 (2011).
[23] R. Nair and M. Gu, Fundamental limits of quantum illumination, Optica **7**, 771 (2020).
[24] H. Yang, N. Samantaray, and J. Jeffers, Quantum illumination with multiplexed photodetection, Phys. Rev. Appl. **18**, 034021 (2022).
[25] Q. Zhuang, Z. Zhang, and J. H. Shapiro, Entanglement-enhanced Neyman–Pearson target detection using quantum illumination, J. Opt. Soc. Am. B **34**, 1567 (2017).
[26] Q. Zhuang, Z. Zhang, and J. H. Shapiro, Entanglement-enhanced lidars for simultaneous range and velocity measurements, Phys. Rev. A **96**, 040304(R) (2017).
[27] E. D. Lopaeva, I. Ruo Berchera, I. P. Degiovanni, S. Olivares, G. Brida, and M. Genovese, Experimental realization of quantum illumination, Phys. Rev. Lett. **110**, 153603 (2013).
[28] Z. Zhang, M. Tengner, T. Zhong, F. N. C. Wong, and J. H. Shapiro, Entanglement's benefit survives an entanglement-breaking channel, Phys. Rev. Lett. **111**, 010501 (2013).
[29] Z. Zhang, S. Mouradian, F. N. C. Wong, and J. H. Shapiro, Entanglement-enhanced sensing in a lossy and noisy environment, Phys. Rev. Lett. **114**, 110506 (2015).
[30] S. Barzanjeh, S. Pirandola, D. Vitali, and J. M. Fink, Microwave quantum illumination using a digital receiver, Sci. Adv. **6**, eabb0451 (2020).
[31] Q. Zhuang, Z. Zhang, and J. H. Shapiro, Optimum mixed-state discrimination for noisy entanglement-enhanced sensing, Phys. Rev. Lett. **118**, 040801 (2017).
[32] S. Guha and B. I. Erkmen, Gaussian-state quantum-illumination receivers for target detection, Phys. Rev. A **80**, 052310 (2009).
[33] Q. Zhuang and J. H. Shapiro, Ultimate accuracy limit of quantum pulse-compression ranging, Phys. Rev. Lett. **128**, 010501 (2022).
[34] Q. Zhuang and S. Pirandola, Ultimate limits for multiple quantum channel discrimination, Phys. Rev. Lett. **125**, 080505 (2020).
[35] Q. Zhuang, Quantum ranging with Gaussian entanglement, Phys. Rev. Lett. **126**, 240501 (2021).
[36] J. Tachella, Y. Altmann, N. Mellado, A. McCarthy, R. Tobin, G. S. Buller, J.-Y. Tourneret, and S. McLaughlin, Real-time 3D reconstruction from single-photon lidar data using plug-and-play point cloud denoisers, Nat. Commun. **10**, 4984 (2019).
[37] P. McManamon, Review of ladar: A historic, yet emerging, sensor technology with rich phenomenology, Opt. Eng. **51**, 060901 (2012).
[38] D. Shin, F. Xu, D. Venkatraman, R. Lussana, F. Villa, F. Zappa, V. K. Goyal, F. N. C. Wong, and J. H. Shapiro, Photon-efficient imaging with a single-photon camera, Nat. Commun. **7**, 12046 (2016).
[39] K. Morimoto, A. Ardelean, M.-L. Wu, A. C. Ulku, I. M. Antolovic, C. Bruschini, and E. Charbon, Megapixel time-gated SPAD image sensor for 2D and 3D imaging applications, Optica **7**, 346 (2020).
[40] S.-Y. Lee, D. H. Kim, Y. Jo, T. Jeong, Z. Kim, and D. Y. Kim, Bound for Gaussian-state quantum illumination using a direct photon measurement, Opt. Express **31**, 38977 (2023).
[41] H. Yang, W. Roga, J. D. Pritchard, and J. Jeffers, Gaussian state-based quantum illumination with simple photodetection, Opt. Express **29**, 8199 (2021).
[42] L. Cohen, E. S. Matekole, Y. Sher, D. Istrati, H. S. Eisenberg, and J. P. Dowling, Thresholded quantum LIDAR: Exploiting photon-number-resolving detection, Phys. Rev. Lett. **123**, 203601 (2019).
[43] H. Liu, D. Giovannini, H. He, D. England, B. J. Sussman, B. Balaji, and A. S. Helmy, Enhancing LIDAR performance metrics using continuous-wave photon-pair sources, Optica **6**, 1349 (2019).
[44] T. Gregory, P.-A. Moreau, E. Toninelli, and M. J. Padgett, Imaging through noise with quantum illumination, Sci. Adv. **6**, eaay2652 (2020).
[45] D. G. England, B. Balaji, and B. J. Sussman, Quantum-enhanced standoff detection using correlated photon pairs, Phys. Rev. A **99**, 023828 (2019).
[46] S. Frick, A. McMillan, and J. Rarity, Quantum rangefinding, Opt. Express **28**, 37118 (2020).
[47] P. S. Blakey, H. Liu, G. Papangelakis, Y. Zhang, Z. M. Léger, M. L. Iu, and A. S. Helmy, Quantum and non-local effects offer over 40 dB noise resilience advantage towards quantum lidar Nat. Commun. **13**, 5633 (2022).
[48] K. M. R. Audenaert, J. Calsamiglia, R. Muñoz-Tapia, E. Bagan, L. Masanes, A. Acin, and F. Verstraete, Discriminating states: The quantum Chernoff bound, Phys. Rev. Lett. **98**, 160501 (2007).
[49] K. Li, Discriminating quantum states: The multiple Chernoff distance, Ann. Stat. **44**, 1661 (2016).
[50] F. Nielsen, An information-geometric characterization of Chernoff information, IEEE Signal Process. Lett. **20**, 269 (2013).
[51] G. Ortolano, E. Losero, S. Pirandola, M. Genovese, and I. Ruo-Berchera, Experimental quantum reading with photon counting, Sci. Adv. **7**, eabc7796 (2021).
[52] G. Ortolano, P. Boucher, I. P. Degiovanni, E. Losero, M. Genovese, and I. Ruo-Berchera, Quantum conformance test, Sci. Adv. **7**, eabm3093 (2021).
[53] J. H. Shapiro, The quantum illumination story, IEEE Aerosp. Electron. Syst. Mag. **35**, 8 (2020).
[54] S. Pirandola, Quantum reading of a classical digital memory, Phys. Rev. Lett. **106**, 090504 (2011).
[55] G. Ortolano and I. Ruo-Berchera, Quantum readout of imperfect classical data, Sensors **22**, 2266 (2022).
[56] C. Helstrom, *Quantum Detection and Estimation Theory* (Academic Press, New York, 1976).
[57] S. Pirandola, R. Laurenza, C. Ottaviani, and L. Banchi, Fundamental limits of repeaterless quantum communications, Nat. Commun. **8**, 15043 (2017).
[58] C. Leang and D. Johnson, On the asymptotics of m-hypothesis Bayesian detection, IEEE Trans. Inf. Theory **43**, 280 (1997).
[59] F. Nielsen, Revisiting Chernoff information with likelihood ratio exponential families, Entropy **24**, 1400 (2022).
[60] See Supplemental Material at http://link.aps.org/supplemental/10.1103/PhysRevResearch.7.L022059 for detailed calculations and additional analysis.